About the inevitable compromise between spatial resolution and accuracy of strain measurement for bone tissue: a 3D zero-strain study

E. Dall'Ara [a, b] *, D. Barber [c], M. Viceconti [a, b]

Affiliations:
[a] Department of Mechanical Engineering, University of Sheffield, Sheffield, UK
[b] INSIGNEO Institute for in silico medicine, University of Sheffield, Sheffield, UK
[c] Department of Cardiovascular Science, University of Sheffield, Sheffield, UK

*Corresponding Author: Enrico Dall'Ara

Department of Mechanical Engineering
INSIGNEO Institute for in silico Medicine
Room C+01-C+ Floor
The Pam Liversidge Building, Sir Frederick Mappin Building
Mappin Street, Sheffield, S1 3JD
United Kingdom
Mobile: 0044 793 6067065
Fax: 0044 114 2227890
Email: e.dallara@sheffield.ac.uk

Word count
Abstract: 246 words
Introduction-Acknowledgements: 3990 words
Appendix: 478
Tables: 1
Figures: 5

ABSTRACT

The accurate measurement of local strain is necessary to study bone mechanics and to validate micro computed tomography (µCT) based finite element (FE) models at the tissue scale. Digital volume correlation (DVC) has been used to provide a volumetric estimation of local strain in trabecular bone sample with a reasonable accuracy. However, nothing has been reported so far for µCT based analysis of cortical bone. The goal of this study was to evaluate accuracy and precision of a deformable registration method for prediction of local zero-strains in bovine cortical and trabecular bone samples. The accuracy and precision were analyzed by comparing scans virtually displaced, repeated scans without any repositioning of the sample in the scanner and repeated scans with repositioning of the samples.

The analysis showed that both precision and accuracy errors decrease with increasing the size of the region analyzed, by following power laws. The main source of error was found to be the intrinsic noise of the images compared to the others investigated. The results, once extrapolated for larger regions of interest that are typically used in the literature, were in most cases better than the ones previously reported. For a nodal spacing equal to 50 voxels (498 µm), the accuracy and precision ranges were 425-692 µε and 202-394µε, respectively. In conclusion, it was shown that the proposed method can be used to study the local deformation of cortical and trabecular bone loaded beyond yield, if a sufficiently high nodal spacing is used.

1 INTRODUCTION

Osteoporotic fractures increase morbidity and mortality, reduce the quality of life, and affect the economy of our ageing society (Kanis and Johnell, 2005). A deep understanding of bone mechanical properties at the different dimensional scales is necessary to develop new diagnostic methods and drug treatments that can be used to reduce the negative outcomes of bone pathologies. In particular, the investigation of the mechanical properties of bone biopsies (10^{-3}-10^{-2} m) is needed in order to understand how much they depend on bone quantity (e.g. bone mineral density, bone volume fraction) and quality (e.g. microarchitecture, morphology, etc.) (Bouxsein, 2003).

At that dimensional scale a number of studies have investigated the relationships between trabecular and cortical bone apparent mechanical properties and their volume fraction, mineral density and microarchitecture (Kaneko et al., 2003; Kopperdahl and Keaveny, 1998; Li et al., 2013; Nyman et al., 2009; Ohman et al., 2007; Wolfram et al., 2011), by means of mechanical testing and micro computed tomography (μCT) scanning. However, little is known about the local distribution of stress and strain of bone under certain loads, information necessary to study how bone structure and its local mechanical competence are related. At the organ level strain gages (Cristofolini et al., 2010; Trabelsi and Yosibash, 2011) and digital image correlation (DIC) techniques (Amin Yavari et al., 2013; Dickinson et al., 2011) have been used to perform strain measurement on a limited portion of the external surface of the tested bone. However, these methods can not be used at the biopsy level, where the space is limited and 3D volumetric information becomes essential due to the complex microstructure.

Yet, another approach that combines repeated μCT images and digital volume correlation (DVC) techniques has been developed recently to study the mechanical behaviour of whole vertebrae (Hussein et al., 2012), trabecular bone (Bay et al., 1999; Bremand et al., 2008; Gillard et al., 2014; Liu and Morgan, 2007; Zauel et al., 2006), scaffolds (Madi et al., 2013) and bone implant interface (Basler et al., 2011). These deformable registration approaches can provide an estimation of the distribution of displacements and strains between two 3D images of the sample before and after a

certain deformation is applied. The information obtained can be used not only to estimate the relationships between bone morphological properties and local deformations, but also to validate the local prediction of μCT based FE models. In this context, it is of fundamental importance to carefully measure the accuracy and precision of this experimental method before any direct application. The precision of the measured displacement and strains with a number of DVC approaches is reported by a number of studies. Conversely, the accuracy is only reported by a few of them (please see the exhaustive literature review by Roberts et al. (2014) and the paper published recently by Gillard et al. (2014)). The different DVC methods applied to trabecular bone led to wide ranges of accuracy and precision for displacement measurements: 0.004–0.272 voxels and 0.005–0.115 voxels (Liu and Morgan, 2007; Zauel et al., 2006), respectively. For strain, the range reported in the literature for accuracy and precision are 20– ~1280με and 39– ~630με (Gillard et al., 2014; Liu and Morgan, 2007; Zauel et al., 2006), respectively (the "~" indicates that the data were extracted from the graphs of the referenced papers). Usually these parameters are estimated by registering repeated scans of the same sample to include errors related to the registration procedure as well as from the intrinsic noise in the μCT image. The large differences in results was probably due to different DVC methods used (such as the dimension of the region of interest, the optimization criterion, the interpolation function, etc.) (Roberts et al., 2014), and the different samples analysed (anatomical site, dimension, etc.) (Liu and Morgan, 2007; Roberts et al., 2014). In particular, it seems that there is a strong dependency between the dimension of the sub-region of interest and both accuracy and precision of the method.

Surprisingly, little is known about the reliability of the method in predicting the local strain of a more homogeneous material such as cortical bone. In fact, in the authors' knowledge, there is only one study where the accuracy of the method is reported for a small portion of the diaphysis of mice femora based on high resolution Synchrotron radiation scans (Christen et al., 2012). However, that study focused on a smaller dimensional scale and did not report accuracy and precision of the method based on repeated measurements. In fact, Christen at al. (2012) found an accuracy close to zero but a very large precision error (up to 13000με), by comparing an original image and its virtual translation of

4

0.5 voxels along each direction. Therefore, such methodology probably underestimates the error introduced in a real case where two different scans are registered, and therefore where the intrinsic noise of the images might play a significant role during the deformable registration. For these reasons, this study was not directly compared to the results of the present study.

The goal of this study was to evaluate the accuracy and precision of a deformable registration method previously used for soft tissues to investigate the local displacements and strains in cortical and trabecular bone samples, in the particular case of zero-strain.

2 MATERIAL AND METHODS

The accuracy of the proposed method to estimate the local strains in µCT images of cortical and trabecular bone samples was estimated by analyzing simulated and real displacement and zero-strain fields (Liu and Morgan, 2007) (Figure 1). In total each sample was scanned three times. After the first original scan (Scan1), the second and third scans were performed without (Scan2) and with (Scan3) repositioning of the sample holder in the machine. The analysis of a simulated displacement was based on the comparison between Scan1 and Scan1 after a virtual translation of two voxels in each direction. This experiment was used to estimate the predicted local total displacement (that should be 3.464 voxels) and the local strains (that should be 0) in an ideal case. Moreover, the accuracy of the method in predicting real strains was estimated by performing two further analyses. Scan1 and Scan2 were compared to estimate the accuracy and precision of the method by including the effect of the noise of the images for repeated scans. Furthermore, Scan2 and Scan3, rigidly registered to Scan2, were compared to evaluate the accuracy by including also a rigid registration (and therefore interpolation) error. In all cases accuracy and precision of the displacement and of the strain were estimated with the mean and standard deviation of the difference between the imposed and measured variables.

2.1 Sample preparation and scanning

Samples were extracted from a bovine femur, collected from animal that was killed for alimentary

purposes. Two sections were cut with a precision diamond saw (*Isomet1000, Buehler, USA*) from the greater trochanter (12mm in thickness) and diaphysis (20mm in thickness) of the femur. A diamond core drill tool mounted on a drilling machine was used to extract under constant water irrigation a 3mm in diameter cylindrical cortical bone sample and an 8mm in diameter cylindrical trabecular bone sample. The samples were then scanned in saline solution with a μCT (*Skyscan 1172, Bruker*) with the parameters reported as following. X-Ray detector: 10 Megapixel 12-bit digital cooled ORCA-HR CCD, 2000x1048 pixels. Voltage equal to 59kV and to 70kV were used for the trabecular and cortical bone, respectively. All the other parameters were the same for both bone types: power equal to 10 W, voxel size equal to 9.96μm (spatial resolution equal to 5 μm), exposure time equal to 1180 ms, rotation step equal to 0.7°, total rotation equal to 180°, images averages x2, 1mm Aluminum beam hardening filter, height scan 9.323mm.

2.2 Image processing

After image reconstruction, a parallelepiped with square cross section of 180x180 voxels and height equal to 932 voxels (9.28mm) was cropped in the central portion of each sample. These dimensions were chosen to fit in the volume of the smaller cortical bone sample (CORT). For comparison with the literature, also a larger region in the trabecular sample was cropped (cube with 430 voxels in each side, equivalent to 4.28mm side length, similar to the one reported by Liu and Morgan (2007)).

To evaluate the effect of a masking operation, the trabecular bone sample (TRAB) was also segmented as following. A mask (binary image with one for bone voxel and zero elsewhere) was created from the original images by applying first a Gauss filter to reduce the noise (sigma equal to 1.5) followed by a single level threshold chosen according to the histograms (Tassani et al., 2011). The quality of the mask was checked by visual inspection. The obtained mask was multiplied to the original image, obtaining a masked trabecular bone sample (TRAB-Masked) with the original greyscale value in the bony pixels, and zero elsewhere.

For the first comparison (Scan1, simulated displacement) a bounding box of ten voxels was added

around the sample that was virtually translated of two voxels in each direction. All cropping and translating steps were done with the free imaging processing toolkit *MeVisLab* (*MeVis Medical Solutions AG*, http://www.mevislab.de/). For the third comparison (Scan2 vs Scan3) the repositioned scan was rigidly registered by using the *MERIT* script in *MeVisLab*. This 3D multi-resolution rigid registration script is based on Sum of Squared Differences (SSD) as similarity measure, and the parameters of the rigid registration were chosen after a proper optimization performed on two 3D images of cortical and trabecular bone virtually rotated and translated of a known quantity (unpublished data).

2.3 Registration and evaluation of displacements

In this study a deformable image registration toolkit (*ShIRT*) (Barber and Hose, 2005; Barber et al., 2007; Khodabakhshi et al., 2013), which was previously applied to soft tissues, was used. We report here only the main steps of the procedure and more details in Appendix1.

The procedure focuses on the recognition of identical features in the two 3D images (called the fixed and moved images). The problem can be translated into finding the displacement functions u, v and w that map each point in the fixed image (with coordinates x, y, z) into the ones in the moved image (with coordinated $x' = x + u$, $y' = y + v$, $z' = z + w$). In ShIRT the mapping function is computed in points of a homogeneous cubic grid superimposed to the images, with nodal spacing NS. The computed displacement functions are then interpolated (tri-linearly) to provide full 3D field estimations of displacement in each point of the image. In this study we have investigated the accuracy and precision of the estimated displacements and strains in function of NS, varied from 5 to 50 voxels (Table1). For the larger images cropped from the trabecular bone sample, also NS equal to 125 and 150 voxels were analyzed.

2.4 Evaluation of Strain

ShIRT computes the displacements at the nodes of the grid. Each grid was then converted into a reticular structure that was defined as a mesh for a FE model. Elements were defined as 8-nodes

hexahedrons. The displacements computed in each point of the grid by ShIRT were then used to define the kinematic boundary conditions in each node of the FE model. The model was then solved linearly (*ANSYS Mechanical APDL v. 14.0, Ansys, Inc., USA*) and the six strain components were computed in each node. For every node the average of the absolute values of the six components of the strain tensor (eAvg) was computed (*Python v. 2.7, Python software foundation*).

2.5 Estimation of accuracy and statistics

The accuracy and precision of the displacement and strain were defined as the mean and SD of the computed displacements and eAvg, respectively. Two-factor analysis of variance with Tukey post hoc tests were performed to compare accuracy of the method for eAvg and computed displacement (factors: NS and structure CORT, TRAB or TRAB-Masked). The analysis was repeated for the three comparisons (translated images, repeated scans and repeated scans with repositioning).

The deformable registration procedure was also checked qualitatively by superimposing the fixed and registered moved images. The two monochromatic images were displayed in MATLAB as the red and green components of a RGB image. The blue component was set to zero. Therefore, the superimposed images appeared in yellow where the registration was successful and in green or red where it was not (Figure 2).

3 RESULTS

The results from the analysis of the simulated displaced image showed an average difference between the displacement measured by the method and the imposed one lower than 0.0004 voxels (for TRAB-Masked, NS=5 voxels), with a standard deviation lower than 0.0233 voxels (for TRAB, NS=5 voxels). For this comparison the accuracy was dependent from NS ($p<0.001$ for both displacement and strain) but not for Structure ($p>0.950$ for both displacement and strain). In particular, both accuracy and precision increased with increasing of the NS for all bone types, both for predictions of displacements and strains. For strains a large error was found with a nodal spacing lower than 15, while with larger NS the accuracy and precision errors were both lower than 30 $\mu\varepsilon$ (Figure 3). The

comparison of repeated scans without repositioning (Scan1 vs Scan2) included the error due to the image noise while comparison of scans with repositioning (Scan2 vs Scan3) included errors due both to noise and to interpolation after a rigid registration was applied. These errors (Figure 4) were larger than the ones computed for simulated displacement (differences of two orders of magnitude).

The accuracy-NS and precision-NS relationships were found to be best approximated to power laws for both cortical and trabecular bone (Figure 5, $R^2 \geq 0.964$). For comparison with the literature the regression curve was extended to larger NS as shown in Figure 5 (sub-figures).

For both comparison between repeated scans (with and without repositioning) the accuracy was found to depend both on structure and on NS (in all cases p<0.001). In particular, accuracy and precision errors were higher for cortical bone than for trabecular bone (differences of 48-14694µε, percentile differences of 8-54%). Similar trends were found for precision (differences of 39-3841µε and percentile differences of 13-46% for precision, all in function of NS). Moreover, differences were also found between trabecular bone and masked trabecular bone samples (p<0.001). In fact, while the accuracy error was substantially lower for the TRAB-Masked compared to the TRAB for low NS (differences of 76-18% for NS=5-15 voxels), it was higher for larger NS (differences of 134-201µε, equivalent to 13-57% for 20≤NS≤50 voxels). Furthermore, comparing the errors in the average strain measured from not-repositioned (Scan1 vs Scan2) or repositioned (Scan2 vs Scan3) images, for NS larger than 15 voxels, smaller differences were found (CORT: difference in error: 4-137µε, percentile difference: 1-8%; TRAB: difference in error: 51-229µε, percentile difference: 11-18%; TRAB-Masked: difference in error: 26-99µε, percentile difference: 4-12%).

Qualitatively, by comparing the superimposed fixed and registered moved images, the errors were uniformly distributed along the whole volume of the sample.

The computational time per CPU (2.9 GHz each), for a pc with 8 GB memory can be estimated as the sum of time needed for the deformable registration with ShIRT (approximately 115 s for NS = 50 voxels to 292s for NS=5 voxels) and of the one for computing the strain with FE (total time 5s for

NS = 50 voxels to 112 s for NS=5 voxels).

4 DISCUSSION

The aim of this study was to investigate the accuracy and sensitivity of a deformable registration method to estimate local zero-strain field in cortical and trabecular bone samples.

The results from the images virtually translated showed that for NS≥20 voxels the errors for the displacements are lower than 0.001 voxels, which translates into accuracy and precision for strains better than 10µε and 20µε. However, when two repeated scans were analyzed, the error increased due to the intrinsic noise of the µCT images. This error dominates the accuracy and precision of the method. Indeed, adding a rigid registration before the analysis did have only a limited impact onto the error (percentile difference range 0.4-28.3%, absolute differences for accuracy lower than 97µε for NS larger than 30 voxels). Therefore, the accuracy and precision of this approach to measure the local strain by combining image registration and µCT scans is mainly affected by the noise of the images, which depends on the scanning parameters and on the µCT hardware.

Furthermore, this study showed for the first time the accuracy and precision of a DVC method applied to µCT images for cortical bone samples. The accuracy was found to be, for most NS values, 10-25% lower than for trabecular bone and a few hundreds µε for a NS larger than 40-50 voxels. Considering that bone yields at 7000-8000µε (Morgan and Keaveny, 2001; Morgan et al., 2001), such accuracy and precision would be sufficient to discriminate the regions that start yielding but in order to study the elastic regime, a larger NS should be used, reducing the ability of describing the local strain close to sub-features of the image. This compromise has to be decided in each single application of the method.

For both cortical and trabecular bone, the relationships between accuracy in the strain and NS were best approximated with power laws. The extrapolation was checked by analyzing two larger sub-regions of the original trabecular bone sample (NS=125 and NS=150 voxels). The small differences between the extrapolated values and the measured ones (43µε for NS=125 voxels and 19µε for

NS=150 voxels) suggest that the power laws are a fair extrapolation of the relationships. The results showed accuracy and precision errors comparable or better than the ones reported in the literature where µCT images were used. Liu and Morgan (2007) used a voxel size equal to 36µm and nodal spacing equal to 40 voxels (equivalent to a NS for our data ~145 voxels) and they found an average error for strain predictions (345-794µm) one order of magnitude larger than the one extrapolated in this study (36µε). In another study, Gillard et al. (2014) did analyze a large trabecular bone samples by using a voxel size equal to 24.6µm and a nodal spacing equal to 64 voxels (equivalent to a NS in the present study of approximately 158 voxels). A big variation in accuracy was reported for repeated scans without (mean strains equal to 20±40µε) or with (250±750µε) an applied rigid translation (repositioning) in between the scans. While the accuracy resulting from the stationary test was slightly better than the one extrapolated in this study (31±31µε for NS=158 voxels), the one computed after repositioning was better in this study (38µε for NS=158 voxels, details not reported here but computed with the same methodology shown for the relationship between repeated scans without repositioning). Similar trends were found for the precision when comparing the one found in this work with the ones reported in the last mentioned studies. The overall improvement in accuracy and precision found in this study might be due to the different deformable registration approach used to compute the displacements and the different scanning machines and parameters used. The results of this study together with the others reported in the literature using different DVC methods (Bay et al., 1999; Gillard et al., 2014; Liu and Morgan, 2007; Zauel et al., 2006) suggest that with the current µCT scanners and registration methods, the accuracy and precision remain pretty constant for NS larger than 70-75 voxels (~700µm) with values lower than 200µε.

Also, the results of this study showed some difference between cortical and trabecular bone samples. The differences in accuracy decrease with increasing of NS. In particular, the difference becomes lower than 100µε for NS larger than 60 voxels. Therefore, it seems that the few features of a typical cortical bone sample, detectable with the resolution used in this study (e.g. Haversian and Volksmann's canals), are sufficient to obtain reasonable strain accuracy and precision for large

enough nodal spacing (in this study around 50 voxels). The procedure used in this study seems to be less affected by the different microstructures compared to results showed by Liu and Morgan (2007), who found ranges of accuracy and precision of the method for trabecular bone samples extracted from different species and anatomical sites wider than the ones found in this study for completely different microstructures as cortical ad trabecular bone (accuracy range: 360-800µε vs 36-51µε; precision range: 130-250µε vs 21-27µε). However, more samples should be analysed to confirm this hypothesis. Furthermore, the masking operation of the trabecular bone provided smaller error for NS lower than 20 voxels and slightly higher errors for larger NS (differences of approximately 150-250µε). These effects might be due to the larger gradients of intensity in the contour of the bone tissues compared to the not masked case (value of marrow equal to 0 for masked, equal to 5000-7000, total greyscale range 0-65535 for 16 bit images) that might work in favour of the registration for small regions of interest and against it for larger NS. Therefore, the masking operation should be avoided when high precision and accuracy in the strains are a requirement. A further rigid registration and tri-linear interpolation did only slightly increase the errors compared to the analysis of the repeated scans.

The potential of this technique is limited by the fact that the accuracy of the zero-strain field measurement is reduced by increasing the spatial resolution of the method. This might be due to: 1) the intrinsic spatial resolution of the machine, and therefore its ability to distinguish features on the two input images, 2) the chosen parameters of the registration algorithm (e.g. the tri-linear interpolation of the displacement output) and 3) a systematic error in the accuracy of the displacement measurements. As small differences in the outcomes of the procedure were found for two completely different microstructures (cortical and trabecular bone), the number of features recognized by the µCT might not be the primary reason. In fact, it is likely that a systematic accuracy error in the displacement would lead to lower error for larger grid size. As analogy, the accuracy of an extensometer in predicting local strains increases when its gage length (i.e. the distance in between the two application points) is increased. However, we do not have at the moment reliable experimental data to prove it and further analysis should be performed to clarify this issue.

This study has one major limitation: only one sample for each bone type was investigated. However, considering the small differences found between images with very different density such as cortical and trabecular bone, the results of this study seems to be quite independent from the bone density and structure. Yet, it would be interesting to analyze samples formed partially by cortical and trabecular bone. In that case, due to the fact that the scanning procedure can not be optimized for both microstructures simultaneously, the images would not have optimal contrast everywhere in the sample. This might affect the signal to noise ratio and secondly the registration accuracy. Further studies will be performed in this direction.

In conclusion, we proposed here to apply a deformable registration method used in the past for soft tissues, to study the local deformation in trabecular and cortical bone samples scanned with μCT. The accuracy and precision of the selected deformable registration method was found to decrease as a power law with increasing nodal spacing. The method seems to be suitable for analyzing the deformation of cortical and trabecular bone samples by using a nodal spacing equal to 600-700μm that would provide both accuracy and precision of approximately 200με for trabecular and cortical bone samples.

5 ACKNOWLEDGEMENTS

REFERENCES:

Amin Yavari, S., van der Stok, J., Weinans, H., Zadpoor, A.A., 2013. Full-field strain measurement and fracture analysis of rat femora in compression test. Journal of Biomechanics 46, 1282-1292.

Barber, D.C., Hose, D.R., 2005. Automatic segmentation of medical images using image registration: diagnostic and simulation applications. J Med Eng&Tech 29, 53-63.

Barber, D.C., Oubel, E., Frangi, A.F., Hose, D.R., 2007. Efficient computational fluid dynamics mesh

generation by image registration. Medical Image Analysis 11, 648-662.

Basler, S.E., Mueller, T.L., Christen, D., Wirth, A.J., Muller, R., van Lenthe, G.H., 2011. Towards validation of computational analyses of peri-implant displacements by means of experimentally obtained displacement maps. Computer Methods in Biomechanics and Biomedical Engineering 14, 165-174.

Bay, B.K., Smith, T.S., Fyhrie, D.P., Saad, M., 1999. Digital Volume Correlation: Three-dimensional Strain Mapping Using X-ray Tomography. Experimental Mechanics 39, 217-226.

Bouxsein, M.L., 2003. Bone quality: where do we go from here? Osteoporososis International 14 Suppl 5, S118-127.

Bremand, F., Germaneau, A., Doumalin, P., Dupre', J.C., 2008. Study of mechanical behavior of cancellous bone by Digital Volume Correlation and R-ray Micro-Computed Tomography. In Proceedings of XIth International Congress and Exposition. Orlando, Florida, USA.

Christen, D., Levchuk, A., Schori, S., Schneider, P., Boyd, S.K., Muller, R., 2012. Deformable image registration and 3D strain mapping for the quantitative assessment of cortical bone microdamage. Journal of Mechanical Behavior of Biomedical Materials 8, 184-193.

Cristofolini, L., Schileo, E., Juszczyk, M., Taddei, F., Martelli, S., Viceconti, M., 2010. Mechanical testing of bones: the positive synergy of finite-element models and in vitro experiments. Philosophical Transactions. Series A .Mathematical Physical and Engineering Sciences 368, 2725-2763.

Dickinson, A.S., Taylor, A.C., Ozturk, H., Browne, M., 2011. Experimental validation of a finite element model of the proximal femur using digital image correlation and a composite bone model. Journal of Biomechanical Engineering 133, 014504.

Gillard, F., Boardman, R., Mavrogordato, M., Hollis, D., Sinclair, I., Pierron, F., Browne, M., 2014. The application of digital volume correlation (DVC) to study the microstructural behaviour of trabecular bone during compression. Journal of the Mechanical Behaviour Biomedical Materials 29, 480-499.

Hussein, A.I., Barbone, P.E., Morgan, E.F., 2012. Digital Volume Correlation for Study of the Mechanics of Whole Bones. Procedia IUTAM 4, 116-125.

Kaneko, T.S., Pejcic, M.R., Tehranzadeh, J., Keyak, J.H., 2003. Relationships between material properties and CT scan data of cortical bone with and without metastatic lesions. Medical Engineering and Physics 25, 445-454.

Kanis, J.A., Johnell, O., 2005. Requirements for DXA for the management of osteoporosis in Europe. Osteoporosis International 16, 229-238. Epub 2004 Dec 2024.

Khodabakhshi, G., Walker, D., Scutt, A., Way, L., Cowie, R.M., Hose, D.R., 2013. Measuring three-dimensional strain distribution in tendon. Journal of Microscopy 249, 195-205.

Kopperdahl, D.L., Keaveny, T.M., 1998. Yield strain behavior of trabecular bone. Journal of Biomechanics 31, 601-608.

Li, S., Demirci, E., Silberschmidt, V.V., 2013. Variability and anisotropy of mechanical behavior of cortical bone in tension and compression. Journal of Mechanical Behaviour of Biomedical Materials 21, 109-120.

Liu, L., Morgan, E.F., 2007. Accuracy and precision of digital volume correlation in quantifying displacements and strains in trabecular bone. Journal of Biomechanics 40, 3516-3520.

Madi, K., Tozzi, G., Zhang, Q.H., Tong, J., Cossey, A., Au, A., Hollis, D., Hild, F., 2013. Computation of full-field displacements in a scaffold implant using digital volume correlation and finite element analysis. Medical Engineering and Physics 35, 1298-1312.

Morgan, E.F., Keaveny, T.M., 2001. Dependence of yield strain of human trabecular bone on anatomic site. Journal of Biomechanics 34, 569-577.

Morgan, E.F., Yeh, O.C., Chang, W.C., Keaveny, T.M., 2001. Nonlinear behavior of trabecular bone at small strains. Journal of Biomechanical Engineering 123, 1-9.

Nyman, J.S., Leng, H., Dong, X.N., Wang, X., 2009. Differences in the mechanical behavior of cortical bone between compression and tension when subjected to progressive loading. Journal of Mechanical Behaviour of Biomedical Materials 2, 613-619.

Ohman, C., Baleani, M., Perilli, E., Dall'Ara, E., Tassani, S., Baruffaldi, F., Viceconti, M., 2007. Mechanical testing of cancellous bone from the femoral head: experimental errors due to off-axis measurements. Journal of Biomechanics 40, 2426-2433.

Roberts, B.C., Perilli, E., Reynolds, K.J., 2014. Application of the digital volume correlation technique for the measurement of displacement and strain fields in bone: A literature review. Journal of Biomechanics 47, 923-934.

Tassani, S., Ohman, C., Baruffaldi, F., Baleani, M., Viceconti, M., 2011. Volume to density relation in adult human bone tissue. Journal of Biomechanics 44, 103-108.

Trabelsi, N., Yosibash, Z., 2011. Patient-specific finite-element analyses of the proximal femur with orthotropic material properties validated by experiments. Journal of Biomechanical Engineering 133, 061001.

Wolfram, U., Wilke, H.J., Zysset, P.K., 2011. Damage accumulation in vertebral trabecular bone depends on loading mode and direction. Journal of Biomechanics 44, 1164-1169.

Zauel, R., Yeni, Y.N., Bay, B.K., Dong, X.N., Fyhrie, D.P., 2006. Comparison of the linear finite element prediction of deformation and strain of human cancellous bone to 3D digital volume correlation measurements. Journal of Biomechanical Engineering 128, 1-6.

Conflict of interest statement:
There is no conflict of interests regarding this paper.

Table 1: Nodal spacing (NS) used for the different registration analysis. For each NS the number of nodes, number of elements and the dimension of the element used in the FE models are reported.

NS [voxels]	Nr Nodes [.]	Nr elements [.]	Dim element [µm]
5	258741	243648	49.8
10	34295	30456	99.6
15	10985	9216	149.4
20	5929	4800	199.2
25	3159	2432	249.0
30	1617	1152	298.8
35	1421	1008	348.6
40	1225	864	398.4
45	575	352	448.2
50	525	320	498.0

Figure 1: Overview of the images used in the project for cortical bone. Same methodology was used for trabecular and trabecular masked images. Each sample was scanned three times, with a repositioning of the sample holder in between the Scan2 and Scan3. The first analysis was performed by registering the cropped region from Scan1 with the same image virtually translated of 2 voxels along each direction. The second analysis was performed by registering the cropped regions from Scan1 and Scan2. The third analysis was performed by registering the cropped region from Scan2 and the cropped region from the Scan3 after a rigid registration with Scan2. The deformable registration provided the field of displacement in the grid defined by the nodal spacing NS and was used to create an FE mesh of hexahedrons the nodes of which were displaced of the values computed by ShIRT. Finally the strains were computed with ANSYS (v. 14.0, Ansys, Inc., USA) and the postprocessing (averaging, plotting, etc.) performed with Python (v. 2.7, Python software foundation).
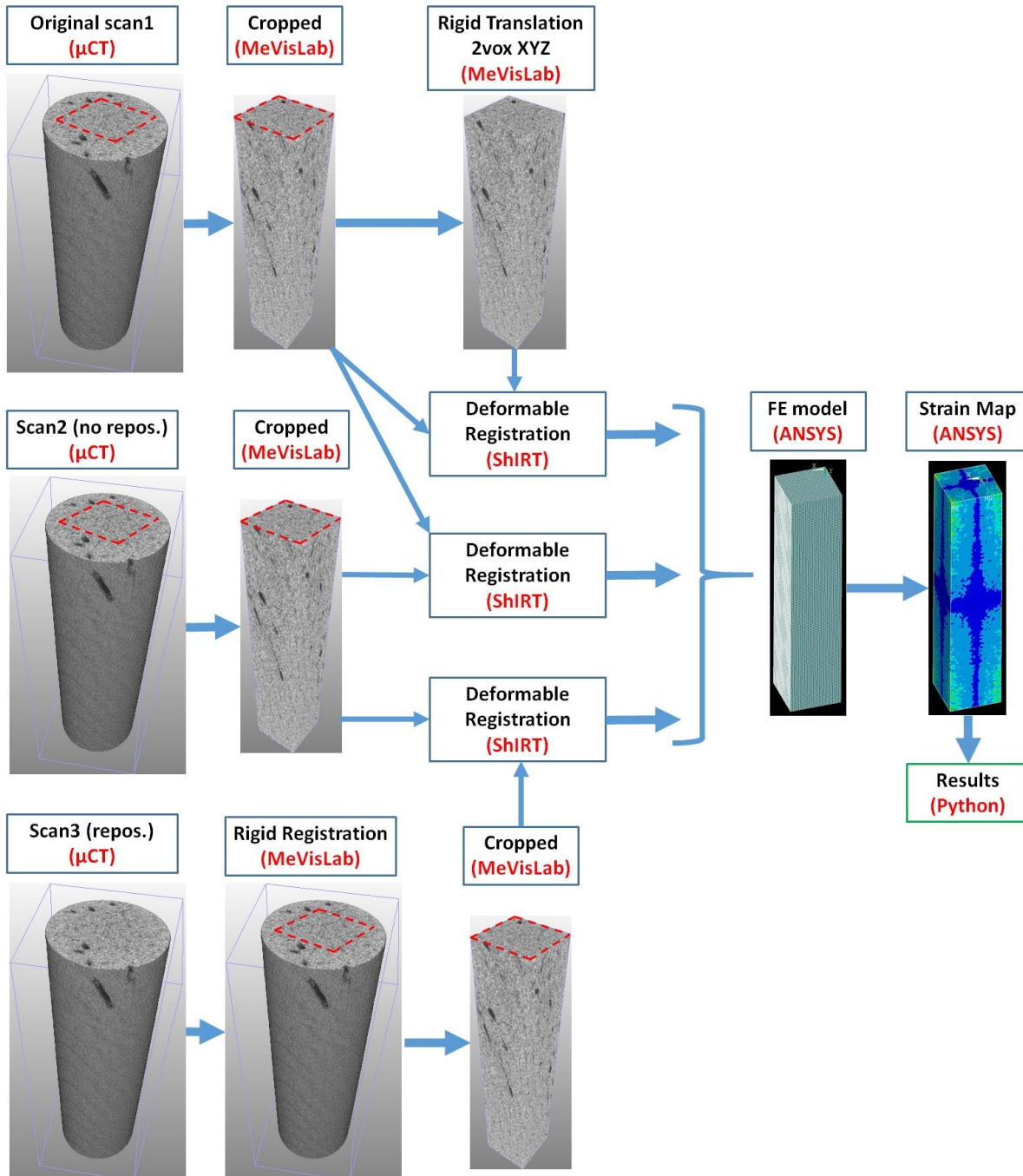
Figure 2: registration grids. The registration was performed on the three types of images and with different nodal spacing $5 \leq NS \leq 50$. The grid, deformed after registration, is overlapped in blue. The images represent the middle cross section of the 3D image computed as superimposion of the fixed (in green) and moved (in red) images. Therefore, the regions well registered are represented in yellow scale. The noise in the registration is homogeneously distributed in the image (for a proper evaluation of the colors please refer to the electronic version of the figure).
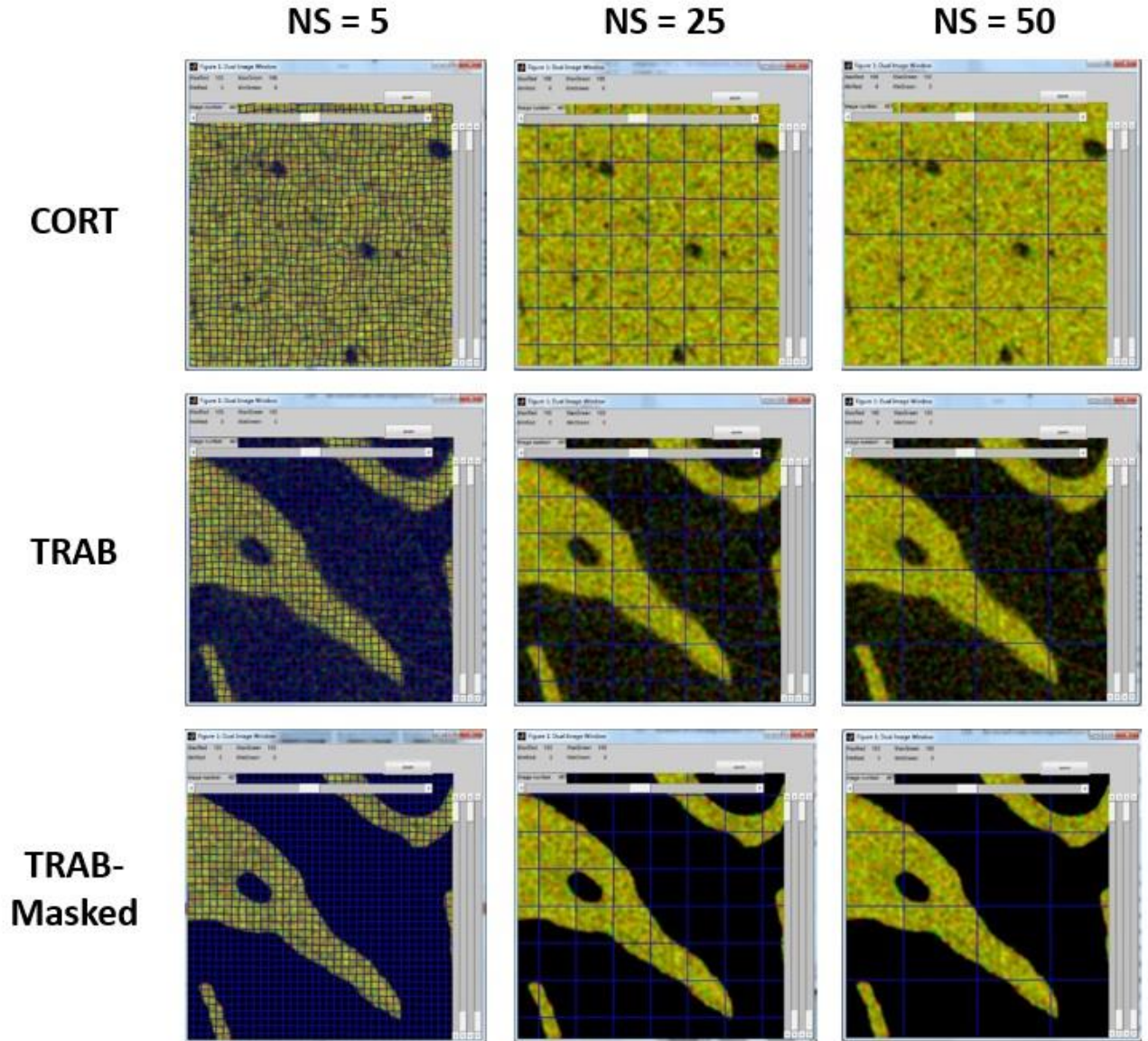
Figure 3: accuracy (above) and precision (below) of the method to evaluate the average strain (eAvg). The accuracy is computed as the average strain computed by registering Scan1 with Scan1 virtually translated of two voxels in each direction.
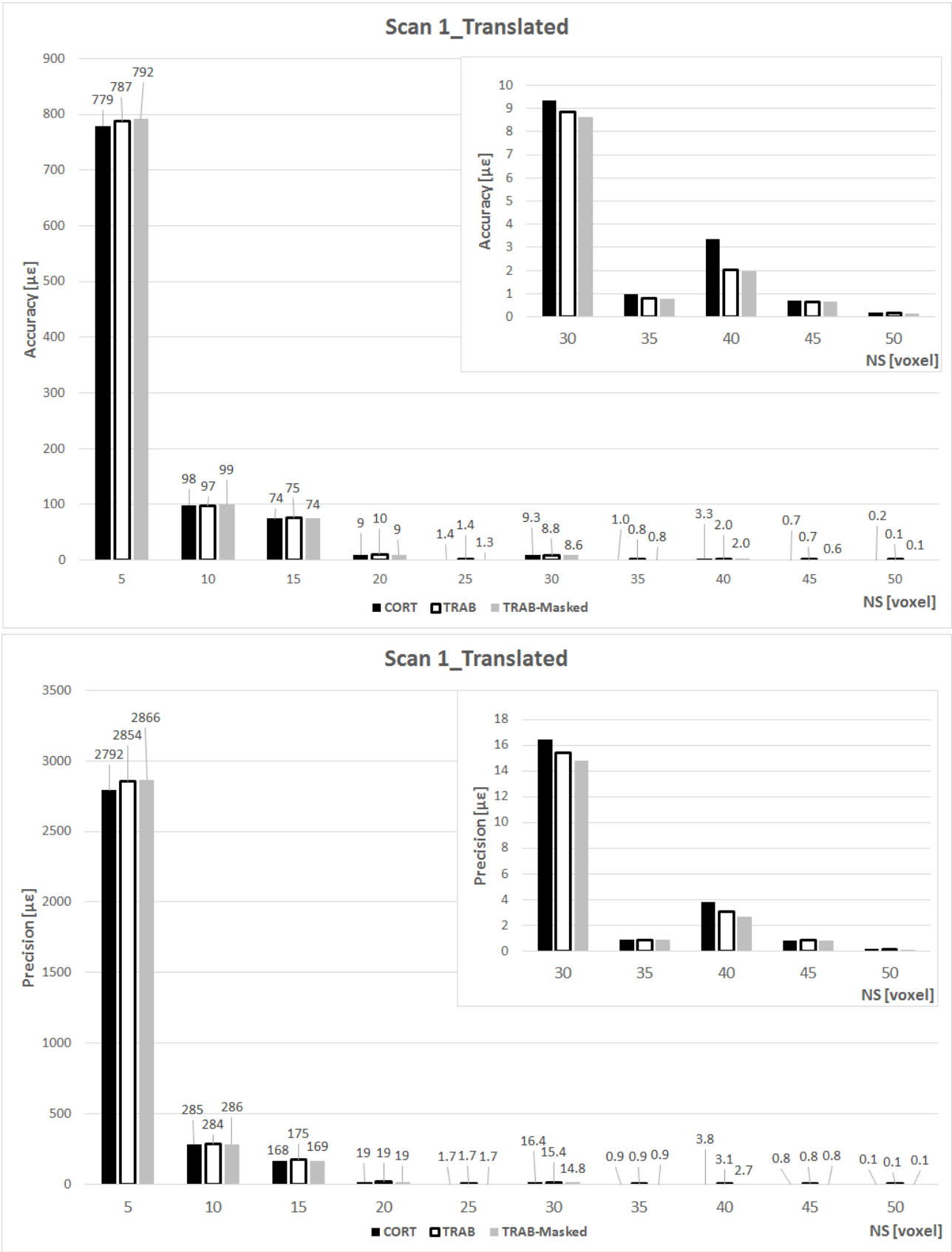
Figure 4: accuracy (above) and precision (below) of the method to evaluate the average strain (eAvg) measured by comparing the repeated scans with (Scan2 vs Scan3; CORT-Reg, TRAB-Reg and TRAB-Masked-Reg) and without (Scan1 vs Scan2; CORT, TRAB, TRAB-Masked) repositioning of the sample holder in between.
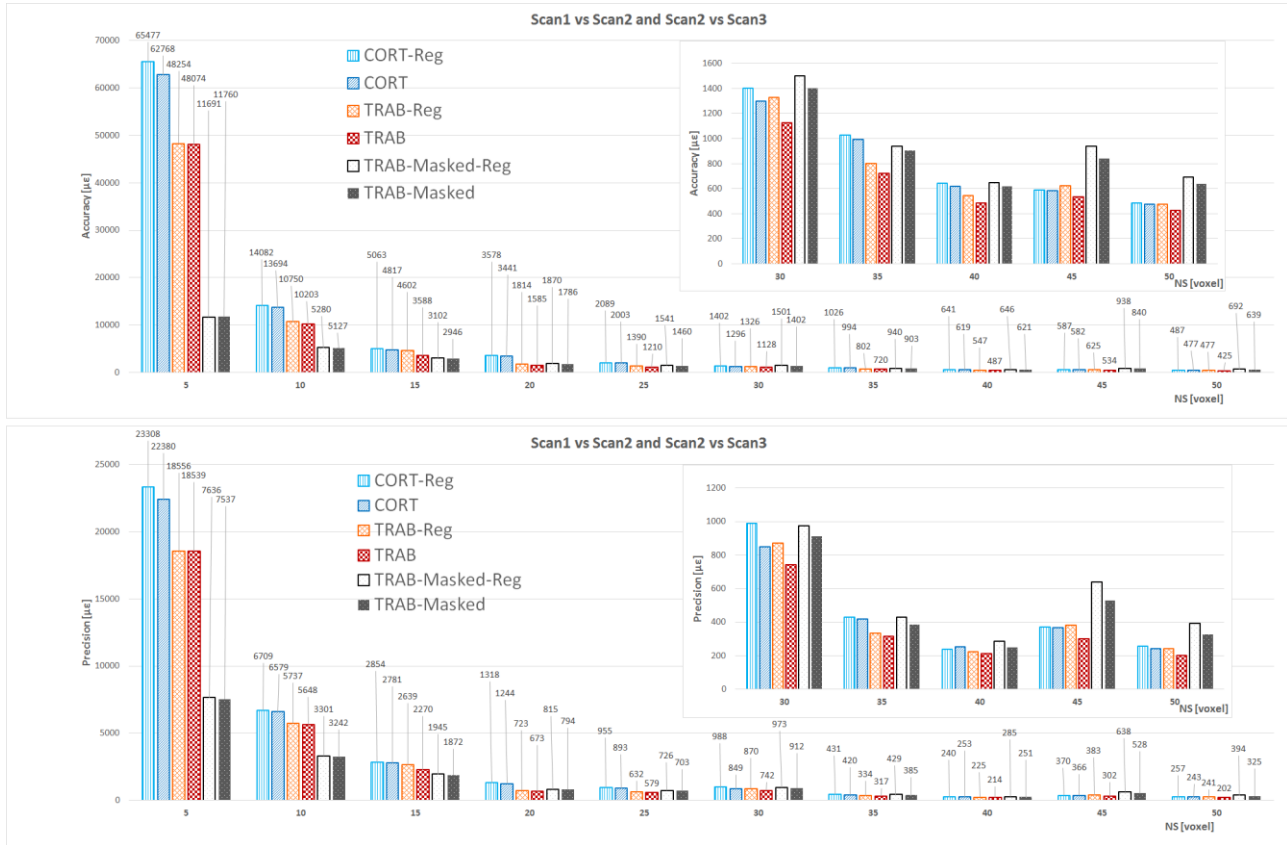
Figure 5: accuracy-NS (above) and precision-NS (below) relationships for the method proposed in this study for cortical (blue) and trabecular (red) bone. The regressions were computed with 5≤NS≤50 for both cortical and trabecular bone. The data were best fitted with power laws. Two larger regions of trabecular bone were included in the sub-graph (open red circles) to check the error committed by taking the extrapolated curve for NS>50. Results from the literature where included in the sub-graphs as well. In that case the NS spacing was computed as product between the NS and the voxel size used in those studies, divided by the voxel size used in this study (9.96 μm). "eAvg6comp" stays for the average of strain computed in each element as the average of the absolute values of the six strain components of the tensor; "HV" = Human Vertebra; "BDF" = Bovine Distal Femur; "BPT" = Bovine Proximal Tibia; "PF" = Proximal femur; "HT" = Human tibia. "Zauel" measured strain on original (II) or smoothed (I) displacement maps. "Gillard_with Tra" means that in that study the deformable registration was applied after a translation of the original image.
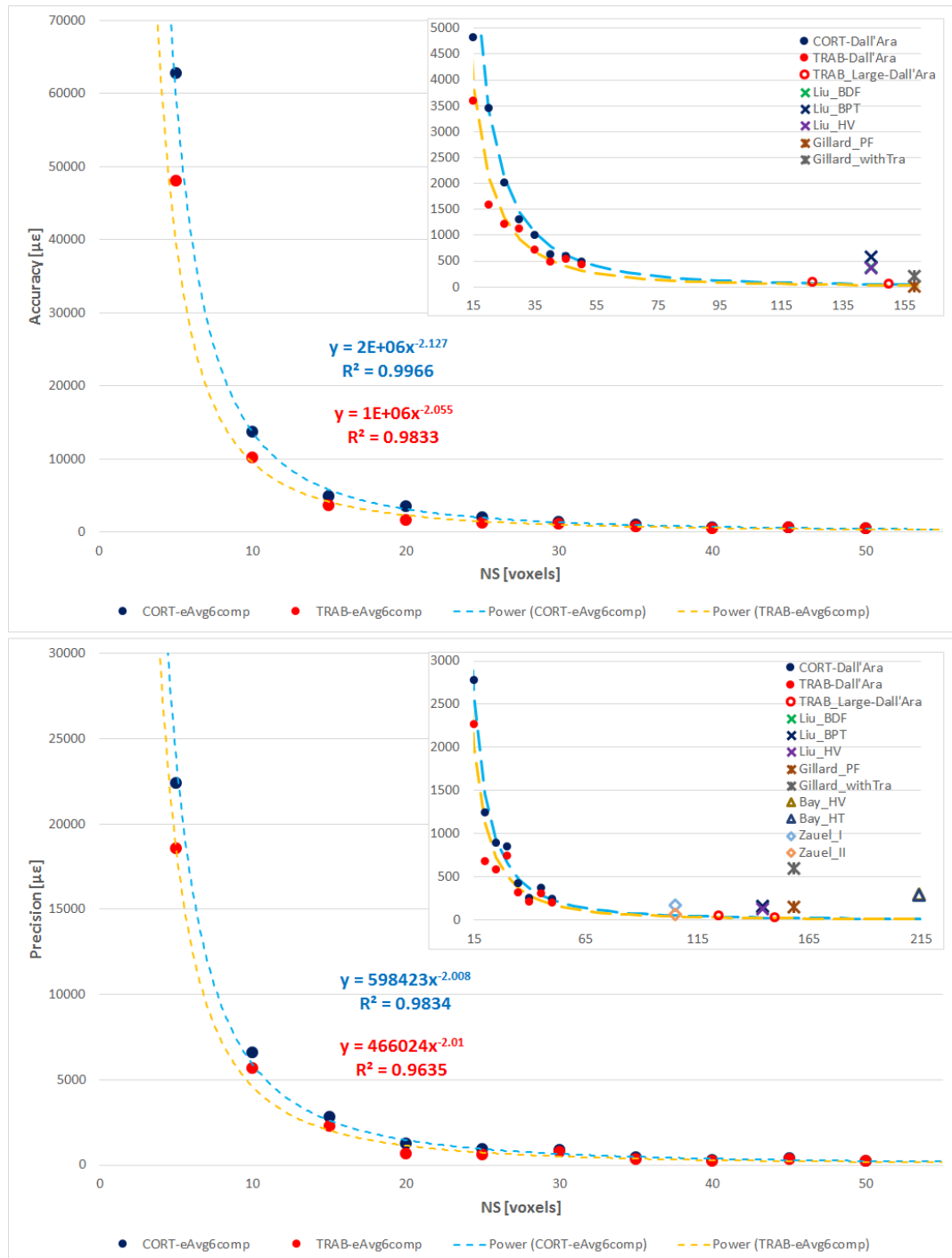
Appendix: Details about the registration algorithm used in this study. More details are reported in Barber et al. (2007).

The detailed description of the registration algorithm is reported in Barber et al. (2007). We report here the main steps.

If we have two images f and m containing similar features we can write a mapping function which maps the coordinates *(x,y,z)* of a feature in f to the coordinates *(x',y',z')* of the same feature in m. These coordinate pairs are related through three displacement functions: *u(x,y,z)*, *v(x,y,z)* and *w(x,y,z)* where:

$$x' = u(x, y, z) + x; \quad y' = v(x, y, z) + y; \quad z' = w(x, y, z) + z$$

The registration problem can be described as finding the mapping function which minimizes the difference between the two images f and m. If the mapping function is represented by the three spatial displacement functions and an additional intensity displacement function *c(x, y, z)* then it can be shown (Barber et al., 2007) that for small displacement values:

$$f(x, y, z) - m(x, y, z) \approx \frac{1}{2}\left(u\left(\frac{\partial f}{\partial x} + \frac{\partial m}{\partial x}\right) + v\left(\frac{\partial f}{\partial y} + \frac{\partial m}{\partial y}\right) + w\left(\frac{\partial f}{\partial z} + \frac{\partial m}{\partial z}\right) - c(f + m)\right)$$

To spatially register the images f and m, the displacements *u*, *v*, and *w* must be computed at each voxel position. One of these equations exists for each image voxel. If there are K voxels, there are K equations but $4K$ unknowns and the resulting set of simultaneous equations is underdetermined. To circumvent this problem a cubic grid with nodal spacing NS voxels is superimposed on the images and a set of tri-linear basis functions centered on the node points defined. The displacement functions are expanded in terms of this set of local basis functions:

$$u(x, y, z) = \sum_i a_{xi} \varphi_i(x, y, z)$$

$$v(x, y, z) = \sum_i a_{yi} \varphi_i(x, y, z)$$

$$w(x, y, z) = \sum_i a_{zi} \varphi_i(x, y, z)$$

The unknowns to be found now become the coefficients "a_{ji}" of the expansions. Provide NS is sufficiently large the resulting set of equations is no longer underdetermined. The set of simultaneous equations can be represented in matrix form as

$$f - m = Ta$$

f and m are vectors of length K. If total number of nodes is N then a is a vector of length 4N. T is a KxN matrix and is derived from integrals of the image gradients multiplied by the basis functions in a straightforward manner.

Unfortunately, although this equation in principle can be solved for T this matrix is generally poorly conditioned and is unlikely to produce robust solutions for a. ShIRT adds an additional constraint which smoothness on the mapping. It is easily shown that the result of adding this constraint is to convert the above equation to the form

$$T^T(f - m) = (T^T T + \lambda L^T L)a$$

where L is a Laplacian operator, and λ is a coefficient that weights the relative importance of smoothing. For suitable values of λ this equation produces robust solutions for $a.$

The second equation is an increasingly poor approximation as displacement values become larger but it is possible to iterate to a correct solution, starting with $a = 0$. If a_n is the value of the displacements after n iterations then the updated values are

$$a_{n+1} = a_n + [T^T T + \lambda L^t L]^{-1} \left(T^T (f - m(a_n)) - \lambda L^t L a_n \right)$$

Iteration continues until the average absolute value of difference between a_{n+1} and a_n is below a tolerance, in this case 0.1 voxels.

REFERENCES

Barber, D.C., Oubel, E., Frangi, A.F., Hose, D.R., 2007. Efficient computational fluid dynamics mesh generation by image registration. Medical Image Analysis 11, 648-662.